

This is the **accepted version** of the article:

Flórez Sarasa, Igor; Obata, Toshihiro; Fernández del Saz, Néstor; [et al.]. «The Lack of Mitochondrial Thioredoxin TRXo1 Affects In Vivo Alternative Oxidase Activity and Carbon Metabolism under Different Light Conditions». *Plant & cell physiology*, (July 2019). DOI 10.1093/pcp/pcz123

This version is available at <https://ddd.uab.cat/record/214287>

under the terms of the  **IN**
COPYRIGHT license

Article type: Regular paper

Title: The lack of mitochondrial thioredoxin TRXo1 affects *in vivo* alternative oxidase activity and carbon metabolism under different light conditions

Running head: Thioredoxin regulation of (photo)respiratory metabolism

Corresponding author: I. Florez-Sarasa; Centre for Research in Agricultural Genomics (CRAG) CSIC-IRTA-UAB-UB, Campus UAB Bellaterra, Barcelona, Spain. Telephone number: +34 9356366 ext 3231; Fax number: +34 935636601; email: igor.florez@cragenomica.es

Subject Areas:

- Photosynthesis, respiration and bioenergetics
- Proteins, enzymes and metabolism

Black and white Figures: 6

Colour Figures: 1

Supplemental Figures: 2

Supplemental Tables: 5

Title: The lack of mitochondrial thioredoxin TRXo1 affects *in vivo* alternative oxidase activity and carbon metabolism under different light conditions

Running head: Thioredoxin regulation of (photo)respiratory metabolism

Igor Florez-Sarasa^{1,5}, Toshihiro Obata^{1,2}, Néstor Fernández Del-Saz^{3,6}, Jean-Philippe Reichheld⁴, Etienne H. Meyer¹, Manuel Rodriguez-Concepcion⁵, Miquel Ribas-Carbo³, Alisdair R. Fernie¹

¹Max-Planck-Institut für Molekulare Pflanzenphysiologie, Am Mühlenberg 1, 14476 Potsdam-Golm, Germany

²University of Nebraska Lincoln, 1901 Vine Street, Lincoln, 68588 NE

³Grup de Recerca en Biologia de les Plantes en Condicions Mediterrànies, Departament de Biologia, Universitat de les Illes Balears, Carretera de Valldemossa Km 7.5, 07122 Palma de Mallorca, Spain

⁴Laboratoire Génome et Développement des Plantes, CNRS, F-66860 Perpignan, France;

⁵Centre for Research in Agricultural Genomics (CRAG) CSIC-IRTA-UAB-UB, Campus UAB Bellaterra, Barcelona, Spain.

⁶Departamento de Botánica, Facultad de Ciencias Naturales y Oceanográficas, Universidad de Concepción, Concepción, Chile.

Author for correspondence: Igor Florez-Sarasa; **Telephone number:** +34 9356366 ext 3231; **Fax number:** +34 935636601; **email:** igor.florez@cragenomica.es

ABSTRACT

The alternative oxidase (AOX) constitutes a non-phosphorylating pathway of electron transport in the mitochondrial respiratory chain that provides flexibility to energy and carbon primary metabolism. Its activity is regulated *in vitro* by the mitochondrial thioredoxin (TRX) system which reduces conserved cysteines residues of AOX. However, *in vivo* evidence for redox regulation of the AOX activity is still scarce. In the present study, the redox state, protein levels and *in vivo* activity of the AOX in parallel to photosynthetic parameters were determined in *Arabidopsis* knock out mutants lacking mitochondrial *trxo1* under moderate (ML) and high light (HL) conditions, known to induce *in vivo* AOX activity. In addition, ¹³C- and ¹⁴C-labeling experiments together with metabolite profiling were performed to better understand the metabolic coordination between energy and carbon metabolism in the *trxo1* mutants. Our results show that the *in vivo* AOX activity is higher in the *trxo1* mutants at ML while the AOX redox state is apparently unaltered. These results suggest that mitochondrial thiol redox systems are responsible for maintaining AOX in its reduced form rather than regulating its activity *in vivo*. Moreover, the negative regulation of the TCA cycle by the TRX system is coordinated with the increased input of electrons into the AOX pathway. Under HL conditions, while AOX and photosynthesis displayed similar patterns in the mutants, photorespiration is restricted at the level of glycine decarboxylation most likely as a consequence of redox imbalance.

Key words: alternative oxidase, mitochondrial thioredoxin, oxygen isotope fractionation, carbon fluxes, high light, *Arabidopsis thaliana*.

INTRODUCTION

The alternative oxidase (AOX) is a terminal oxidase located in the plant mitochondrial electron transport chain (mETC) which constitutes a pathway of electron transport alternative to the cytochrome oxidase (COX) pathway that is mainly responsible for mitochondrial ATP synthesis (Moore and Siedow, 1991). The non-phosphorylating nature of AOX has raised many questions about its function in plants many of them which are focused on the possibility that it balances cellular energy and carbon metabolism under environmental perturbations (Rasmusson *et al.*, 2009; Vanlerberghe, 2013). In order to gain insight into how this protein is regulated, early studies reported *in vitro* properties of AOX such as post-translational modifications (Millar *et al.*, 1993; Umbach and Siedow, 1993). Plant AOX protein exists in a dimeric state that can be redox regulated through a disulfide/sulphydryl system (Umbach and Siedow, 1993). This system allows the reversible formation of disulfide bonds between adjacent monomers of the AOX dimer leading to a covalently-linked inactive dimer or a non-covalently linked active AOX dimer. Once in its reduced (active) state, the AOX activity can be stimulated on interaction with α -ketoacids including pyruvate (Millar *et al.*, 1993; Umbach and Siedow, 1994; Millar *et al.*, 1996; Selinski *et al.*, 2017). Studies in isolated mitochondria reported a significant activity of the AOX after its reduction and addition of pyruvate even when less than 30% of the ubiquinone (UQ) is in its reduced state (Millar *et al.*, 1993; Umbach and Siedow, 1994; Millar *et al.*, 1996). At this UQ reduction state the COX pathway is not fully saturated, therefore, these *in vitro* regulatory features indicated that the AOX pathway can compete with the COX pathway for the electrons of the UQ pool (Hoefnagel *et al.*, 1995; Ribas-Carbo *et al.*, 1995). Competition between the COX and AOX pathways was definitively demonstrated with measurements of the individual activities of both pathways by using the oxygen-isotope fractionation technique (Ribas-Carbo *et al.*, 1995; 1997). It is currently well accepted that the *in vivo* activities of both the AOX and COX pathways can be determined by the oxygen-isotope fractionation technique while inhibitors can only be used for measuring AOX and COX capacities (Ribas-Carbo *et al.*, 2005; Del-Saz *et al.*, 2018).

The two regulatory features described above are currently considered as the main post-translational mechanisms responsible for plant AOX activation, although the extent to which these mechanisms affect its activity *in vivo* still remains as a matter of debate (Riemer *et al.*, 2015; Del-Saz *et al.*, 2018). The AOX has generally been only detected in

its reduced-active form in whole tissue extracts, a fact often interpreted to imply that redox regulation is unlikely to occur *in vivo* (Millenaar and Lambers, 2003). However, Noguchi *et al.* (2005) showed that the AOX activity can be regulated by its reduction state in leaves of *Alocasia odora* (a shade species) under different light conditions. Moreover, in different C3 species, post-translational regulation of AOX has recently been shown to be responsible for inducing AOX activity *in vivo* after high light (HL) treatment (Florez-Sarasa *et al.*, 2016). Previous observations suggest that an increase in the levels of NADPH inside mitochondrial matrix would favor the reduction of AOX through the action of a thioredoxin/thioredoxin (TRX) reductase system (Gray *et al.*, 2004). Indeed, there is evidence that the TRX system can modulate AOX reduction state and enhance AOX capacity in the mitochondria isolated from leaves of poplar (Gelhaye *et al.*, 2004), pea (Marti *et al.*, 2009) and Arabidopsis (Yoshida *et al.*, 2013). However, aside from studies in isolated mitochondria, whether AOX is indeed regulated by the TRX system *in vivo* is still unclear (Geigenberger *et al.*, 2017).

The plant mitochondrial TRX system consists of NADPH-dependent TRX reductases and mitochondrial TRXs (Laloi *et al.*, 2001; Reichheld *et al.*, 2005; Geigenberger *et al.*, 2017). The *TRXo1* gene has been confirmed to encode a mitochondrial TRX while its paralog *TRXo2* is expressed at very low levels and its localization has not yet been confirmed (Meyer *et al.*, 2012). Poplar *PtTrxh2* has been shown to be in mitochondria while its ortholog in Arabidopsis, *AtTrxh2*, is found not only in the cytosol and mitochondria (Meng *et al.*, 2009; Meyer *et al.*, 2012) but also in the endoplasmic reticulum and Golgi (Traverso *et al.*, 2013). Moreover, addition and activation of recombinant TRXo1 protein to isolated mitochondria induces the thiol redox switch of the AOX protein in Arabidopsis, pea and thermogenic skunk cabbage (Marti *et al.*, 2009; Yoshida *et al.*, 2013; Umekawa and Ito, 2018). Therefore, the use of genetically modified *TRXo1* plants is a promising approach to test the *in vivo* function of the mitochondrial TRX system. In this respect, biochemical analyses of *trxo1* T-DNA mutants in Arabidopsis have already been proven highly useful in unraveling the regulatory mechanisms by which the TRX-system regulates TCA cycle enzymes *in vivo* (Daloso *et al.*, 2015; Yoshida and Hisabori, 2016).

In the present study, we examined the response of *trxo1* knock-out mutants on shifting from moderate light (ML) to high-light (HL) which has previously been reported to induce *in vivo* AOX activity. For this purpose, we measured *in vivo* AOX and COX leaf

activities, photosynthetic parameters, AOX capacity, protein levels and redox state, relative rates of the TCA cycle and other respiratory fluxes, leaf metabolite profile and ^{13}C label redistribution following incubation with ^{13}C -glucose and ^{13}C -malate. The aims of these experiments were (i) to determine the impact of deficiency of the mitochondrial TRX on the regulation of the *in vivo* AOX activity under ML and HL conditions and (ii) to explore the influence of the mitochondrial TRX on respiratory fluxes and primary metabolism under ML and HL conditions. The TRXo1 has been proposed as the physiological candidate for redox activation of the AOX based on *in vitro* results (Marti et al., 2009; Yoshida et al., 2013; Umekawa and Ito, 2018). In this respect, we report for the first time the *in vivo* AOX activity in plants lacking of *trxo1* under different light conditions. Furthermore, changes on photorespiration were observed under HL conditions denoting the relevance of TRXo1 on the interaction between mitochondrial redox and carbon metabolism under light stress conditions. All these observations are discussed on the basis of the changes on central carbon metabolic fluxes.

RESULTS

TRXo1 inactivation leads to slight changes in the expression of other TRX-related genes and growth impairment

The T-DNA insertion within the *TRXo1* gene was confirmed in both mutant lines (*trxo1-1* and *trxo1-2*) using genomic PCR with T-DNA-specific primers and seeds from homozygous lines were used for subsequent experiments. The insertions in the *TRXo1* gene in both *trxo1-1* and *trxo1-2* lines have previously been mapped and resulted in KO of gene expression (Daloso et al., 2015; Yoshida and Hisabori, 2016). Here, we have confirmed the suppression of *TRXo1* expression in both lines by quantitative PCR analyses (Supplementary Figure S1A). The transcript levels of other genes related to the mitochondrial TRX system were slightly but significantly increased in both mutants (*NTRA*) or only in *trxo1-2* (*TRXo2* and *TRXh*) (Supplemental Figure S1A). In addition, we analysed the transcript levels of *AOX1a* which encodes the most abundant and redox-sensitive AOX isoform; similar levels were observed in all genotypes. After 6 weeks of growth, the rosettes of mutant lines were smaller than wild-type *Col-0* rosettes (Supplemental Figure S1B), thus displaying a significant ($P<0.05$) 12% and 22% reduction in total rosette fresh weight (Supplemental Figure S1C).

Respiratory activities of AOX and COX pathways under moderate and high light conditions

Total respiration (V_t) and oxygen-isotope fractionation was measured in order to determine the *in vivo* activities of AOX and COX pathways. V_t was significantly increased after 2 and 4 hours of high light (HL) treatment in all lines (Figure 1A) and reached similar activity in all genotypes. Under moderate light (ML) conditions, *trxo1-1* line displayed significantly ($P < 0.05$) higher V_t than *Col-0* plants and *trxo1-2* line also displayed a similar trend (Figure 1A). The *in vivo* activity of COX pathway (v_{cyt}) was also increased after the HL treatment in all lines and no significant differences were observed between *Col-0* and mutant lines at any light condition (Figure 1B). As for the *in vivo* activity of AOX pathway (v_{alt}), a different HL induction pattern was observed between mutant and *Col-0* plants (Figure 1C). The v_{alt} was significantly increased after HL treatment in *Col-0* plants but not in the mutants (Figure 1C). While v_{alt} was similar in all genotypes following HL treatment, both mutant lines displayed higher v_{alt} than *Col-0* plants under ML conditions but does not further increase under HL conditions (Figure 1C).

AOX capacity, protein levels and redox state

We measured the AOX pathway capacity (V_{alt}), i.e. as respiration in the presence of cyanide, as well as AOX protein levels and its redox state in order to further investigate the causes of the altered *in vivo* AOX activities (v_{alt}) -i.e. measured in the absence of inhibitors by oxygen-isotope fractionation. Unlike the v_{alt} , the V_{alt} was similar among genotypes under ML conditions (Figure 2A). In order to evaluate the AOX protein levels in the different genetic backgrounds, we performed immunoblots using anti-AOX antibodies (Figure 2B). The AOX antibody used detects both AOX1 and 2-type isoforms from Arabidopsis (see further information in Material and Methods). After porin levels correction (see Material and Methods for details), the AOX protein levels were similar among genotypes under ML conditions (Figure 2B). On the other hand, the AOX capacity and protein levels were not significantly increased after HL treatment in any of the genotypes (Figure 2). In general, results clearly show that the capacity to respire via AOX

was not altered in the mutants at any light condition and was not induced after HL treatment. Moreover, the percentage of the ratio between activity and capacity of the AOX (previously defined by others as AOX engagement and here calculated from Figure 1C and Figure 2A data) indicates that AOX was engaged at $75 \pm 7\%$ (mean \pm SE) in *Col-0* plants while it was fully engaged in the mutants ($107 \pm 12\%$ and $111 \pm 11\%$). These results suggest that inactivation of *TRXo1* altered the AOX regulation.

In order to further study the AOX regulation, the redox state of the AOX protein was analyzed in isolated leaf membranes with or without the addition of DTT or diamide (Figure 3 and Supplemental Figure S2B, see Material and Methods for details). The AOX monomeric (reduced) and dimeric (oxidized) forms were detected in the presence of DTT and diamide, respectively (Figure 3 and Supplemental Figure S2B). After porin levels correction, the total amount of AOX was similar between genotypes but significantly different between redox treatments, being the mean of the total AOX amount in non-treated, diamide-treated and DTT-treated samples of 0.57 ± 0.04 , 0.13 ± 0.02 and 1.28 ± 0.28 , respectively. Therefore, the redox treatments significantly affected the mitochondrial protein extracted. The reason for these differences remain uncertain, however, these results do not affect to the evaluation of the AOX redox state among genotypes in the non-treated samples. In the absence of redox chemicals, the AOX was mainly found in its monomeric (reduced) form, thus representing 89 to 93% of the total AOX detected in all genotypes (Figure 3 and Supplemental Figure S2B). Signals of the dimeric forms, one with a lower molecular weight perhaps indicating heterodimers from different isoforms, were only between 7% and 11% of the total AOX detected in all genotypes (Figure 3 and Supplemental Figure S2B). Porin levels were very similar among genotypes thus indicating similar mitochondrial loading. Therefore, it is concluded that inactivation of *TRXo1* does not modify the redox state of AOX (Figure 3 and Supplemental Figure S2B).

Respiratory CO₂ evolution for TCA cycle and other respiratory flux analysis under moderate light conditions

In order to determine whether changes on the *in vivo* AOX activity are linked to the other respiratory fluxes the evolution of $^{14}\text{CO}_2$ was recorded following incubation of leaf discs in positionally labeled [^{14}C]glucose. Leaf discs were supplied with [$1\text{-}^{14}\text{C}$]glucose and

[3:4-¹⁴C]glucose over the period of 4 h and evolved ¹⁴CO₂ was determined at hourly interval. The radioactivity released from position C1 of glucose is attributed to decarboxylation processes in the oxidative pentose phosphate pathway and the TCA cycle. The CO₂ released from positions C3:4 is due to the action of pyruvate dehydrogenase or malic enzyme and derived from mitochondrial respiration. The CO₂ evolution from the C1 position of glucose to that from C3:4 position indicates relative respiratory flux through the TCA cycle in relation to other respiratory processes (Kruger et al., 2017). Mutant lines displayed lower CO₂ emission from [1-¹⁴C] glucose, being those differences significant in *trxo1-2* after 3 and 4 hours of incubation (Figure 4). On the other hand, CO₂ emission from [3:4-¹⁴C] glucose was similar in all lines (Figure 4). When ratios between both emissions are calculated, both mutant lines showed higher C3:4 to C1 ratios than *Col-0* plants, being significantly higher in *trxo1-2* and *trxo1-1* lines after 3 and 4 hours, respectively (Figure 4). These results suggest that mutants display higher TCA cycle flux in relation to other respiratory pathways.

Photosynthetic and photorespiratory parameters under moderate and high light conditions

Changes in photosynthesis and photorespiration could cause growth and respiratory metabolism alterations in the *trxo1* mutants. Therefore, gas exchange and chlorophyll fluorescence measurements were performed in fully expanded leaves of all three lines at ML and HL conditions. Net photosynthesis (A_N), stomatal conductance (g_s) and chloroplast electron transport rate (ETR) were higher at HL than at ML conditions in all three lines (Figure 5). Photosynthetic parameters were similar in all lines at HL conditions, with the exception of A_N at 4h of HL which was significantly lower in *trxo1-1* (Figure 5). By contrast, ETR in both mutants and A_N in *trxo1-1* were significantly lower than in *Col-0* plants under ML conditions (Figure 5), although differences were not physiologically relevant. Finally, A_N was measured at saturating light conditions under normal and low O₂ concentration in all genotypes and treatments. The percentage of O₂ inhibition of A_N was then calculated as an indication of photorespiration. Results indicate a significantly lower photorespiration in both mutants under 2h of HL as compared to *Col-0* plants, while similar values among lines were observed at the other light conditions (Figure 5).

262

263 *Metabolite profiles and ^{13}C enrichment analysis under moderate and high light*
264 *conditions*

265 In order to further investigate the metabolic changes underlying the altered responses of
266 (photo) respiratory pathways in the mutants, GC-TOF-MS metabolite profiling analysis
267 was performed on samples harvested under the different light conditions. A total of 36
268 metabolites were annotated after GC-TOF-MS analyses (Table S1) and their relative
269 levels were normalized to the mean levels of *Col-0* plants under ML conditions. Leaves
270 of *Col-0* plants displayed significant increases in 23 and 28 metabolites after 2 and 4 hours
271 of HL treatment, respectively (Figure 6 and Table S2). The greatest fold-change was
272 observed in glycine levels (20 to 37 fold increase) followed by glutamine (10 to 20 fold
273 increase). Metabolite levels in the mutants displayed very similar patterns after HL
274 treatment as compared to *Col-0* plants (Figure 6). Indeed, only trehalose displayed
275 significantly lower levels in both mutant lines after 2h of HL treatment as compared to
276 *Col-0* plants, while isoleucine and threonine levels were higher only in the *trxo1-2* line
277 (Figure 6 and Table S2). On the other hand, the levels of fumarate and *myo*-inositol were
278 consistently lower in both mutant lines under ML conditions (Figure 6), while threonate
279 and 1,4-lactone galactonate levels were lower only in *trxo1-2* mutants.

280 Changes on the relative levels of metabolites are not always linked to changes in
281 metabolic flux (Ferne and Stitt, 2012). In order to have a better estimation of metabolic
282 fluxes in the respiratory pathways, the total ^{13}C label redistribution in different
283 metabolites was determined after 2 and 4 hours of ^{13}C -Glucose and ^{13}C -Malate labeling
284 under ML ($100\ \mu\text{mol m}^{-2}\text{ s}^{-1}$ in this case) and HL ($400\ \mu\text{mol m}^{-2}\text{ s}^{-1}$ in this case) conditions
285 (Figure 7 and Tables S3 and S4). Under ML conditions, most metabolites showed an
286 increase in ^{13}C enrichment after 2 and 4 hours of ^{13}C -Glc feeding (Tables S3 and S4) but
287 only fumarate (in both mutants) and glycine (in *trxo1-1*) displayed statistically higher ^{13}C
288 redistribution in mutants as compared to *Col-0* plants (Figure 7A and Table S3). Higher
289 ^{13}C label redistribution to glycine was also observed after ^{13}C -Mal feeding in *trxo1-2*
290 while label redistribution to fumarate was similar in all genotypes (Figure 7A and Table
291 S4). In addition, increased label redistribution to GABA was observed in both mutants as
292 compared to *Col-0* plants after 4 h of ^{13}C -Mal feeding (Figure 7A). By contrast, decreased
293 label redistribution to *myo*-inositol was observed in *trxo1-1* and *trxo1-2* mutants

following 2h and 4h of ^{13}C -Mal feeding, respectively (Figure 7A). Raffinose and alanine displayed some lower label redistribution only in *trxol-1* after 2h of ^{13}C -Mal feeding under ML conditions (Table S4). The ^{13}C label redistribution in some metabolites was much higher after HL treatment than under ML conditions, however, this was not consistent across the different mutant lines or time points (Tables S3 and S4). Fumarate (^{13}C -Glc feeding), proline (^{13}C -Glc feeding), tryptophan (^{13}C -Mal feeding) and glucose (^{13}C -Mal feeding) displayed significant changes in label redistribution after HL treatment only in single mutant lines and time points (Tables S3 and S4). However, higher label redistribution to glycine following ^{13}C -Mal feeding was consistently observed in both mutant lines and time points (Figure 7B). Moreover, higher label redistribution to glycine after ^{13}C -Glc feeding was also observed in both mutant lines, though at different time points (Figure 7B). Similarly, higher label redistribution to serine was detected in both lines following 2 and 4h of HL treatment of ^{13}C -Glc and ^{13}C -Mal feeding, respectively. Higher label redistribution to alanine and erythritol was detected in both mutant lines following ^{13}C -Glc (2h) and ^{13}C -Mal (4h) feeding, respectively (Figure 7B).

DISCUSSION

The mitochondrial TRXo1 is not required for the AOX activation in vivo

Here we investigated the *in vivo* role of the mitochondrial TRX in the regulation of AOX by combining measurements of the *in vivo* AOX activity in leaves of Arabidopsis mutants lacking mitochondrial *TRXo1* with a range of other physiological analysis. The TRX system has been shown to regulate the AOX activity *in vitro* by reducing conserved Cys thus yielding an active and non-covalently linked AOX homodimer (Gelhaye *et al.*, 2004; Marti *et al.*, 2009; Yoshida *et al.*, 2013). Therefore, the *in vivo* AOX activity was anticipated to be down-regulated in the mutants as compared to *Col-0* plants but surprisingly, our results clearly demonstrate that this is not the case (Figure 1). *In vivo* AOX activity was detected in both mutant lines under ML and HL conditions (Figure 1) at similar or higher levels than in *Col-0* plants. While, these observations suggest that mitochondrial thioredoxin *TRXo1* is not required for the activation of the AOX *in vivo*, we cannot rule out that redox activation of the AOX is being carried out by other thioredoxins or by other thiol reductases (e.g. glutaredoxins) located in the mitochondria (Meng *et al.*, 2009; Moseler *et al.*, 2015). The increased transcript levels of *NTRA*, *TRXh2*,

and *TRXo2* in the *trxo1* mutants may involve possible compensation effects (Figure S1A). Candidate mitochondrial TRXs are *TRXh2* and *TRXo2* which were suggested to be located in mitochondria (Meng *et al.*, 2009; Yoshida and Hisabori, 2016), although direct evidence of their presence in the matrix is still scarce. Further studies involving genetic approaches using multiple mutants of the different redox systems would be required to confirm a compensation effect, which would explain why both reduced and oxidized forms of the AOX were similar in all genotypes (Figure 3 and Supplemental Figure S2B). Nevertheless, evidence against the *in vivo* relevance of the redox regulation of AOX activity has been reported mainly based on the fact that the AOX protein has been detected in its reduced state in different tissues, species and experimental conditions (Del Saz *et al.*, 2018 and references therein). Recently, the oxidized form of the AOX has not been detected neither in *Col-0* nor in *trxo1* mutant *Arabidopsis* plants by using a different redox approach in enriched mitochondrial fractions (Sanchez-Guerrero *et al.*, 2019). While oxidized forms were detected here, the AOX was mainly detected in its reduced form in both in *Col-0* and *trxo1* mutant leaves (Figure 3 and Supplemental Figure S2B). In agreement with our hypothesis, Nietzel *et al.* (2017) have recently suggested that the thiol redox switch of the AOX which operates *in vitro* does not necessarily imply any regulatory function *in vivo* but may rather play an important maintenance function in the avoidance of AOX oxidation.

Vanlerberghe *et al.* (1999) previously suggested that the presence of reduced AOX is necessary for its activity but other factors such as α -ketoacids and the redox state of the UQ pool are critical to ensure AOX activity *in vivo*. Changes in the level of reduced UQ have subsequently been revealed as a key factor explaining AOX activity *in vivo* but importantly not the only factor (Millenaar *et al.*, 2001). The alteration of the different regulatory factors individually (i.e. by using genetically modified plants with altered synthesis of UQ) in combination *in vivo* AOX activity measurements will be key to precisely determine the impact of UQ levels on AOX regulation. The regulation of AOX via interaction with α -ketoacids has also been questioned given that mitochondrial levels of pyruvate have been estimated to be high enough to fully activate AOX (Millenaar and Lambers, 2003). However, increased pyruvate levels and AOX *in vivo* activity were observed in soybean roots following treatment with an inhibitor of branched-chain amino acid biosynthesis (Gaston *et al.*, 2003). Additionally, evidence for pyruvate stimulation of AOX capacity was reported in tubers of transgenic potato with decreased pyruvate

kinase activity (Oliver *et al.*, 2008) and in pea mesophyll protoplasts following high light treatment (Dinakar *et al.*, 2010).

AOX activity is upregulated in vivo by the lack of mitochondrial TRX

Perhaps even more unexpected than the presence of AOX activity is that activity was higher in the *trxo1* mutants than in *Col-0* plants (Figure 1). The higher *in vivo* AOX activity in the mutants consequently reduced the energetic efficiency of respiration. This finding, but not the minor changes observed in photosynthetic carbon assimilation (Figure 5), could explain the rosette growth retardation (Figure 1B). A detailed analysis on adenylate levels in different subcellular compartments (Krueger *et al.*, 2009; Gardeström and Igamberdiev, 2016) would be required at different growth stages to establish the importance of the mitochondrial ATP synthesis efficiency on the mutants growth. On the other hand, *myo*-inositol levels were consistently reduced in both *trxo1* mutants as well as displaying a lower label redistribution to this metabolite, which can indicate a different use of raffinose family oligosaccharides as carbon sources (Van den Ende, 2013). In agreement, Sanchez-Guerrero *et al.* (2019) has recently found a very similar decrease in *myo*-inositol levels in *trxo1* mutants, while also marked decreases in sugar levels were observed. The metabolic differences observed in Sanchez-Guerrero *et al.* (2019) are probably related to the growth of the plants in the presence of sucrose-containing media. Nevertheless, both metabolic phenotypes are in line with an up-regulation of the respiratory metabolism (Sanchez-Guerrero *et al.*, 2019). In addition, the percentage of germination was previously observed to be unaffected in the *trxo1* mutants in the absence of sucrose and stress (Daloso *et al.*, 2015; Ortiz-Espin *et al.*, 2017), similar to the case in the present study. An increased AOX expression in *trxo1* mutants could explain a higher *in vivo* activity of the AOX under ML. However, the AOX capacity and protein levels clearly show that the capacity to respire via AOX was not higher in the mutants than in *Col-0* plants (Figure 2). The AOX capacity (i.e. the rate of oxygen uptake following cyanide inhibition) is well-documented to correlate well with AOX protein abundance but frequently does not correlate with the *in vivo* activity (i.e. as determined with the O₂ isotope technique in the absence of inhibitors, Del-Saz *et al.* (2018) and references therein). Furthermore, the AOX activity and capacity were similar in the mutants under ML conditions (Figure 1C and Figure 2A) indicating that the AOX was running at its full capacity in the mutants. These observations suggest that lack of TRXo1 activates the

AOX protein *in vivo*. A direct redox regulation of the *in vivo* AOX activity by the TRXo1 is, however, unlikely since we could not detect changes in the redox state of the AOX in *trxo1* mutants as compared to *Col-0* plants (Figure 3 and Supplemental Figure S2B).

As a cause for the observed increased *in vivo* AOX activity we alternatively propose an indirect effect of the lack of TRXo1. Our results indicate a higher ratio of TCA cycle to other respiratory fluxes in both mutant lines as compared to the *Col-0* (Figure 4), thus confirming the previously reported negative regulation of the TCA cycle by TRX system (Daloso *et al.*, 2015). In particular, Daloso *et al.* (2015) reported that succinate dehydrogenase (SDH) and fumarase (FUM) activities were higher in TRX mutants. These previous observations could explain the lower levels of fumarate observed in both mutant lines (Figure 6). Note that no change in fumarate but increased malate accumulation was previously reported in TRX mutant leaves at the end of the day (Daloso *et al.*, 2015), while the lower levels of fumarate observed here correspond to analyses of leaf samples at the start of the day. Despite lower fumarate levels, higher ¹³C label redistribution to fumarate was detected in both mutants after ¹³C-Glc labeling. In addition, the higher ¹³C label redistribution to GABA after ¹³C-Mal labeling suggests an increased GABA shunt activity likely in order to replenish succinate levels in the TRX mutants. Taken together, these observations support an increased TCA cycle flux (i.e. from succinate to malate) which provides extra electrons into UQ pool of the electron transport chain and explains the higher AOX *in vivo* activity in *trxo1* mutants under ML conditions. In fact, the higher *in vivo* AOX activity probably maintained the UQ reduction level stable in the *trxo1* mutants, as it is the main general role of AOX (Millenaar and Lambers, 2003; Del-Saz *et al.*, 2018). The similar transcript levels of *AOX1a* observed in *Col-0* and mutant plants supports this view, because *AOX1a* levels are very sensitive and responsive to UQ reduction levels and its ROS associated signals (Rasmusson *et al.*, 2009).

Metabolic adjustments observed in TRX mutants under HL treatment

Lower levels of trehalose were consistently found in both *trxo1* mutants after 2h of HL treatment as compared to *Col-0* plants (Figure 6). Similarly, trehalose levels were lower in *trxo1* mutants after salinity treatment as compared to *Col-0* plants (Sanchez-Guerrero *et al.*, 2019). These concomitant results denotes a specific altered response of trehalose metabolism in the *trxo1* mutants under stress. Trehalose has protection roles against

several abiotic stresses by stabilizing membranes, proteins and other cellular components as well as protecting against ROS (Lunn *et al.*, 2014). Nevertheless, understanding on the trehalose changes observed in the *trxo1* mutants deserve further investigation given that some of the protective roles attributed to trehalose under stress are questioned while others emerge on sugar signaling (Lunn *et al.*, 2014). On the other hand, higher label redistribution to glycine and serine was also consistently observed in both *trxo1* mutants under HL treatment (Figure 7). These results can be explained by a direct effect of TRX on glycine decarboxylase (GDC) activity. Indeed, GDC has been reported as a putative target of the TRX system (Balmer *et al.*, 2004) and its activity in isolated mitochondria can be regulated by the glutaredoxin system (Hoffmann *et al.*, 2013). However, *in vivo* evidence in plants is still missing. In cyanobacteria, the P-protein of the GDC has been proposed to be redox regulated through the formation of a disulfide bond between Cys972 in the C terminus and Cys353 located in the active site (Hasse *et al.*, 2013). Here, glycine and serine ¹³C labeling data suggest a reduced photorespiratory flux *in vivo* in the *trxo1* mutants under HL conditions. Moreover, the lower O₂ inhibition of photosynthesis observed in the mutants after 2h of HL treatment supports this view (Figure 5). The fact that decreased photorespiration was not observed after 4h of HL treatment might indicate the activation of other mechanisms for the dissipation of the reductants at longer time exposition to the stress. Nevertheless, short-term transitions to high light have been recognized as frequent physiological transitions in which mitochondrial metabolism is able to rapidly respond to support photosynthetic activity (Finkemeier and Schwarzländer, 2018). Moreover, a restriction in photorespiration in *AOX1a* mutants has recently been reported by similar decreases in O₂ inhibition of photosynthesis as observed in here and also coinciding with high glycine to serine ratios (Zhang *et al.*, 2017). Therefore, our gas exchange data together with our data on metabolite levels and ¹³C redistribution strongly suggest a restriction on photorespiration in the *trxo1* mutants at the level of glycine decarboxylation.

As discussed above, the higher AOX *in vivo* activity observed in *trxo1* mutants is probably due to an increased activity of the TCA cycle. Photorespiratory activity increases mitochondrial NAD(P)H/ NAD(P) ratios in illuminated leaves which can inhibit the activities of TCA cycle NAD(P)H dehydrogenases (Igamberdiev and Gardeström, 2003), thus altering the operation of the TCA cycle (Sweetlove *et al.*, 2010). Because of these redox links between mitochondrial dehydrogenases, it is unsurprising that the

observed alterations in the TCA cycle reactions in the TRX mutants could affect glycine decarboxylation. In contrast to ML conditions, total respiration and AOX activity *in vivo* were similar in *Col-0* and mutants plants after HL treatment, and all genotypes displayed a full engagement of AOX (i.e. activity was essentially equivalent to capacity). The HL-induction of the *in vivo* AOX activity can be impeded if AOX capacity is limiting; this was observed as a species-specific feature (Florez-Sarasa *et al.*, 2016) and also in *Arabidopsis* plants with *AOX1a* suppression (Florez-Sarasa *et al.*, 2011). In the last case, plants were exhibiting a full AOX engagement already under ML (Florez-Sarasa *et al.*, 2011) as was the case for the *trxo1* mutants in present study. As a consequence of this capacity limitation, the induction of the *in vivo* AOX activity was prevented in the *trxo1* mutants and thus the reoxidation of the extra reductants produced by the TCA cycle under HL. The extra reducing power produced by *trxo1* mutants under HL conditions could then be the cause for the glycine decarboxylation restriction.

Concluding remarks

The *in vivo* AOX activity was higher in *trxo1* mutants under moderate light conditions, as compared to *Col-0* plants, in spite of lacking *TRXo1* which has been proposed to redox activate the AOX (Marti *et al.*, 2009; Yoshida *et al.*, 2013; Umekawa and Ito, 2018). Moreover, we did not detect differences on the redox state of the AOX protein between the mutant and *Col-0* plants. These observations together with the increased transcript levels of other TRX-related systems in the *trxo1* mutants suggest that the AOX is maintained in its reduced state by different mitochondrial redox systems rather than being actively regulated. In addition, the combined analysis of *in vivo* fluxes of the electron transport chain and the TCA cycle has allowed us to better understand the regulation of mitochondrial metabolism from a broader and unprecedented perspective under different light conditions. The *in vivo* AOX activity was increased in *trxo1* mutants thus yielding a fully engaged AOX which was linked to an up-regulation of the TCA flux. Such a higher and less efficient respiration might be the cause of the lower biomass accumulation in *trxo1* mutants, although more detailed analysis of the energy status at different subcellular compartments (Krueger *et al.*, 2009; Gardeström and Igamberdiev, 2016) would be required to unravel this issue. After high light treatment, the *trxo1* mutants displayed a restricted photorespiration at the level of glycine decarboxylation possibly by the lack of AOX response and excess of reductant power in the mitochondrial matrix.

490

491 MATERIAL AND METHODS

492 *Plant material and growth conditions*

493 The Arabidopsis (*Arabidopsis thaliana*) mutants *trxo1-1* and *trxo1-2* were isolated from
494 T-DNA insertion lines SALK_042792 and SALK_143294, respectively, obtained from
495 the Arabidopsis Biological Resource Centre. Genotyping of *trxo1* mutants was performed
496 by PCR using gene- and T-DNA-specific primers as previously described (Daloso *et al.*,
497 2015; Ortiz-Espín *et al.*, 2017). Selected homozygous seeds from both mutant lines were
498 used for all the experiments. Mutant and wild type Columbia-0 (*Col-0*) plants were grown
499 in soil under short photoperiod (8h light/16h dark) and controlled temperature
500 (22°C/18°C), relative humidity (above 60%) and light intensity (150 $\mu\text{mol m}^{-2} \text{s}^{-1}$), which
501 was considered the moderate light (ML) treatment unless otherwise noted. Plants were
502 grown for 6 to 7 weeks under ML and then transferred to high light conditions (600 μmol
503 $\text{m}^{-2} \text{s}^{-1}$) for 2 and 4h, which was considered the high light (HL) treatment unless otherwise
504 noted.

505

506 *Gene expression analysis*

507 RNA was isolated from lyophilized leaves by using Maxwell® RSC Plant RNA Kit
508 (Promega) and automated system Maxwell® RSC Instrument (Promega) according to the
509 manufacturer's instructions, and was quantified using a NanoDrop 1000
510 spectrophotometer (Thermo Scientific, <http://www.nanodrop.com/>). Afterwards cDNA
511 synthesis was performed following the recommendations of the Transcriptor First Strand
512 cDNA Synthesis Kit (Roche). Relative mRNA abundance was evaluated by quantitative
513 PCR using LightCycler 480 SYBR Green I Master Mix (Roche) on a LightCycler 480
514 real-time PCR system (Roche). Primers used and the related information are detailed in
515 the Supplemental Table S5. Two technical replicates of each biological replicate were
516 performed, and the mean values were used for further calculations. Arabidopsis UBC
517 (At5g25760) was used as a reference gene to correct for differences in the total amount
518 of transcripts and the $2^{-\Delta\Delta\text{Ct}}$ method (Livak and Schmittgen 2001) was used to calculate
519 the fold change of gene expression. Finally, data were normalized to the mean value of

Col-0 plants in moderate light conditions (i.e. the level of all transcripts for *Col-0* at moderate light was set to 1).

Measurements of respiratory oxygen consumption and isotope fractionation

Measurements of oxygen consumption and isotope fractionation during respiration were performed as described by Florez-Sarasa *et al.* (2007) in order to determine the *in vivo* activities of the COX and AOX pathways in Arabidopsis leaves. As for the end-point fractionation values, the oxygen isotope fractionation of the AOX pathway was determined after incubation with 10 mM KCN as described previously (Florez-Sarasa *et al.*, 2007) and a mean value of 31.1‰ was used from all the measurements performed both in the mutant and *Col-0* plants because no differences were observed between genotypes. On the other hand, an end-point value of 20.9‰ corresponding to the oxygen isotope fractionation of the COX pathway was taken from previous measurements in Arabidopsis leaves (Florez-Sarasa *et al.*, 2007). Calculations of the electron partitioning and the activities of the AOX and COX pathways were performed following Guy *et al.* (1989). In addition, the AOX capacity was determined with a Clark-type oxygen electrode as described previously (Florez-Sarasa *et al.*, 2009). Five replicates (each representing a different plant) per line and light treatment were performed for both *in vivo* activities and AOX capacity.

Western Blot analysis

For determining the total amount of AOX, 20 mg of frozen leaf powder per genotype and light condition were used for protein extraction directly in 100 µl SDS sample buffer [2% (w/v) SDS, 62.5mM Tris-HCl (pH 6.8), 10% (v/v) glycerol and 0.007% (w/v) bromophenol blue] including 50 mM DTT and protease inhibitor (Roche). Samples were incubated 30 min at 4°C to allow full reduction of the AOX protein and then boiled (95°C) for 5 min. For the analysis of the AOX redox state, leaf membranes were isolated as described in Noguchi *et al.* (2005) with the following modifications. Five leaves (approx. 500 mg) per genotype under moderate light condition were ground with a mortar and pestle in 1 mL of grinding medium (0.45 M mannitol, 50 mM TES, 0.5% (w/v) BSA, 0.5% (w/v) PVP-40, 2 mM EGTA, 20 mM ascorbate) containing either 50 mM DTT (for

AOX reduction), 50 mM diamide (for AOX oxidation) or nothing else. After approx. 1 min of grinding, samples were centrifuged for 5 min at 1200 g and supernatant was transferred into a new tube and centrifuged at 10000g for another 5 min. Subsequently, supernatant was discarded and the pellet was resuspended in SDS sample buffer containing DTT or diamide at the same concentrations as those used during the extraction. Both, extracts for total amount and redox state determinations of the AOX protein were frozen at -20°C.

Twenty microliters were loaded and separated on 12% and 10% SDS-PAGE gels for the total amount and redox state samples, respectively. Proteins were transferred to nitrocellulose membranes using wet Mini-PROTEAN system of Bio-Rad for the total amount samples; PVDF membranes and PeqLab mini gel system was used for the redox samples. The following primary antibodies and dilutions were used for detecting mitochondrial proteins: monoclonal anti-Porin, voltage-dependent anion channel porin (PM035, from Dr Tom Elthon, Lincoln, NE) at 1:5000 dilution; polyclonal anti-AOX, alternative oxidase 1 and 2 (AS04054, Agrisera, Sweden) at 1:500 dilution (used for the total AOX amount); monoclonal anti-AOX (AOA, from Dr Tom Elthon, Lincoln, NE) at a dilution 1:10000. Secondary antibodies linked to horseradish peroxidase were used (Sigma-Aldrich Co.). The signals were detected by chemiluminescence using Pierce™ ECL Western Blotting Substrate (ThermoFischer) and a Luminescent Image Analyzer (G-Box-Chemi XT4, Syngene). The protein band quantifications were performed with GeneTools analysis software from the Luminescent Image Analyzer (G-Box-Chemi XT4, Syngene) according to manufacturer's instructions. The obtained band intensities for AOX were corrected for their corresponding porin band intensities and then normalized to the levels of the *Col-0* plants under moderate light. Four different immunoblot experiments per protein were performed with similar results.

Measurements of respiratory CO₂ evolution

Ten leaf discs with 10 mm diameter were incubated in a 100 ml flask containing 5 mL of 10 mM MES (pH 6.5) under moderate light intensity at room temperature for 30 min prior to the addition of [1-¹⁴C]glucose or [3:4-¹⁴C]glucose (6.2 MBq mmol⁻¹) to a final concentration of 1.0 mM. Each flask was then sealed with Parafilm and shaken at 100 rpm. Evolved ¹⁴CO₂ was collected in 0.5 ml of 10% (w/v) KOH in a 1.5 ml

microcentrifuge tube suspended in the flask. The KOH solution was replaced every hour for 4 h. Radioactivity evolved as CO₂ was determined as the radioactivity in the KOH solution mixed with 4 mL of scintillation cocktail (Rotizint Eco Plus, ROTH) measured by a liquid scintillation counter (LS6500, Beckman Coulter; Kühn et al., 2015). The yield of ¹⁴CO₂ was calculated by expressing the cumulative radioactivity released (Kruger et al., 2017).

Metabolite profiling

Metabolite extractions were performed as described previously (Lisec et al., 2006) using approximately 50 mg of frozen-powdered leaf tissue. Derivatization and gas chromatography-time of flight-mass spectrometry (GC-TOF-MS) analyses were carried out as described previously (Lisec et al., 2006). Metabolites were identified manually by TagFinder software (Luedemann et al., 2008) using the reference library mass spectra and retention indices housed in the Golm Metabolome Database (<http://gmd.mpimp-golm.mpg.de>; Kopka et al., 2005). The parameters used for the peak annotation of the 36 metabolites can be found in Table S1 which follows the reporting recommendations of Fernie et al. (2011). Data were normalized to the mean value of *Col-0* plants in moderate light conditions (i.e. the value of all metabolites for *Col-0* at moderate light was set to 1). Values presented are means ± SE of seven replicates which were taken from same rosettes used for photosynthesis and respiration analyses.

Measurements of the ¹³C isotope redistribution

Leaves of similar size from the *Col-0* and mutant plants were fed via the petiole by placing in a solution containing 10 mM MES-KOH (pH 6.5) and either 15 mM [U-¹³C] Glucose or 15mM [U-¹³C] Malate (from Cambridge Isotope Laboratories) for 4 h. Leaves under control and high light treatments were subjected to 100 and 400 μmoles m⁻² s⁻¹, respectively, so that an approx. the light intensities applied during the petiole feeding were lower than in the other experiments in order to avoid leaf wilting induced by the high transpiration occurring during the high light treatment. Four fold-increase in light intensity during the high light treatment was maintained as in the other experiments. At 0, 2 and 4h of incubation and light treatment, leaves were snap-frozen in liquid nitrogen.

Thereafter, approx. 30 mg of frozen-powdered leaf tissue was extracted and derivatized as described above and analyzed by GC-TOF-MS in parallel with a mixture of authentic standards of several metabolites at four different concentrations. The peak intensity matrix containing all available mass isotopomers of characteristic mass fragments generated by TagFinder was then processed using the CORRECTOR software tool ([http://www.mpimp-golm.mpg.de/10871/Supplementary Materials](http://www.mpimp-golm.mpg.de/10871/Supplementary_Materials)) in order to correct for the natural abundance of the isotope and to calculate the fractional enrichment (Huege *et al.*, 2014). Absolute concentrations were determined for all the metabolites detected and present in the authentic standards mixture. The total ^{13}C label redistributed in a metabolite pool was calculated by multiplying the fractional enrichment with the absolute concentration of the corresponding metabolite.

Leaf gas exchange and chlorophyll fluorescence measurements

Net CO_2 assimilation (A_N), stomatal conductance (g_s) and chlorophyll fluorescence were measured simultaneously with an open infrared gas-exchange analyser system (Li-6400; Li-Cor Inc., Lincoln, NE, USA) equipped with a leaf chamber fluorometer (Li-6400-40, Li-Cor Inc.). Fully expanded leaves were clamped and leaf chamber conditions were set to: $400 \mu\text{mol CO}_2 \text{ mol}^{-1} \text{ air}$ (C_a), temperature of 23°C and photosynthetically active photon flux density (PPFD) of 150 and $600 \mu\text{mol m}^{-2} \text{ s}^{-1}$ (provided by the light source of the Li-6400 with 10% blue light) at moderate light and after high light treatment, respectively. After approx. 3 min, gas-exchange and chlorophyll fluorescence measurements were performed in the light. The actual quantum efficiency of the photosystem II (PSII)-driven electron transport (ΦPSII) and the electron transport rate (ETR) were determined as previously described in Florez-Sarasa *et al.* (2011) except that 0.5 and 0.84 values were used for leaf absorptance and the partitioning of absorbed quanta between photosystems I and II. Six replicates per genotype and light treatment were performed in leaves of different plants.

In addition, A_N was measured at saturating light conditions (PPFD of $1000 \mu\text{mol m}^{-2} \text{ s}^{-1}$) under photorespiratory (21% O_2) and non-photorespiratory (approx. 2% O_2) conditions in all genotypes and treatments. The percentage of O_2 inhibition of A_N was calculated in order to obtain an estimation of photorespiratory activity as previously described (Ku and

645 Edwards, 1977): $\%(A_{N\ 2\%O_2} - A_{N\ 21\%O_2})/ A_{N\ 2\%O_2}$. Four replicates per genotype and light
646 treatment were performed in leaves of different plants.

647

648 *Statistical analyses*

649 Student's t-tests were used for statistical analyses in all the figures and tables in order to
650 compare *trxo1* mutants to the *Col-0* plants in each light treatment and also to compare
651 different high light conditions to the moderate light condition in each genotype.

652

FUNDING

This work was supported by the Alexander von Humboldt Foundation and by the Spanish Ministry of Economy and Competitiveness, through the “Severo Ochoa Programme for Centres of Excellence in R&D” 2016–2019 (SEV - 2015 - 0533)” (I.F.-S.). N.F.D-S. and Miquel R-C. were supported by Spanish Ministries MICINN (BFU2011-23294) and MINECO (CTM2014-53902-C2-1-P). J.-P.R. was supported by the Centre National de la Recherche Scientifique and the Agence Nationale de la Recherche ANR-Blanc Cynthiol 12-BSV6-0011.

DISCLOSURES

The authors declare no conflict of interest.

ACKNOWLEDGEMENTS

We would like to thank Danilo M. Daloso for his helpful discussions and comments on the manuscript. Also thanks to Yunuen Avalos Padilla for helping with Western Blot analyses. And finally we are also very grateful to Dr Biel Martorell at the Serveis Científico-Tècnics of the Universitat de les Illes Balears for his help while running IRMS experiments.

REFERENCES

Balmer Y., Vensel W.H., Tanaka C.K., Hurkman W.J., Gelhaye E., Rouhier N., Jacquot J.P., Manieri W., Schürmann P., Droux M., Buchanan B.B. (2004) Thioredoxin links redox to the regulation of fundamental processes of plant mitochondria. *Proceedings of the National Academy of Sciences of the United States of America* 101: 2642-2647.

Daloso D.M., Müller K., Obata T., Florian A., Tohge T., Bottcher A., Riondet C., Bariat L., Carrari F., Nunes-Nesi A. *et al.* (2015) Thioredoxin, a master regulator of the tricarboxylic acid cycle in plant mitochondria. *Proceedings of the National Academy of Sciences of the United States of America* 112: 1392–1400.

Del-Saz N.F., Ribas-Carbo M., McDonald A.E., Lambers H., Fernie A.R., Florez-Sarasa I. (2018) An *in vivo* perspective of the role(s) of the alternative oxidase pathway. *Trends in Plant Science* 23: 206-219.

Dinakar C., Raghavendra A.S., Padmasree K. (2010) Importance of AOX pathway in optimizing photosynthesis under high light stress: role of pyruvate and malate in activating AOX. *Physiologia Plantarum* 139: 13-26.

Fernie A.R., Stitt M. (2012) On the discordance of metabolomics with proteomics and transcriptomics: coping with increasing complexity in logic, chemistry, and network interactions. *Plant Physiology* 158: 1139-1145.

Florez-Sarasa I., Araujo W.L., Wallstrom S.V., Rasmusson A.G., Fernie A.R., Ribas-Carbo M. (2012) Light-responsive metabolite and transcript levels are maintained following a dark-adaptation period in leaves of *Arabidopsis thaliana*. *New Phytologist* 195: 136-148.

Florez-Sarasa I., Flexas J., Rasmusson A.G., Umbach A.L., Siedow J.N., Ribas-Carbo M. (2011) *In vivo* cytochrome and alternative pathway respiration in leaves of *Arabidopsis thaliana* plants with altered alternative oxidase under different light conditions. *Plant Cell and Environment* 34: 1373-1383.

Florez-Sarasa I., Ostaszewska M., Galle A., Flexas J., Rychter A.M., Ribas-Carbo M. (2009) Changes of alternative oxidase activity, capacity and protein content in leaves of *Cucumis sativus* wild-type and MSC16 mutant grown under different light intensities. *Physiologia Plantarum* 137: 419-426.

Florez-Sarasa I.D., Bouma T.J., Medrano H., Azcon-Bieto J., Ribas-Carbo M. (2007) Contribution of the cytochrome and alternative pathways to growth respiration and maintenance respiration in *Arabidopsis thaliana*. *Physiologia Plantarum* 129: 143-151.

Florez-Sarasa I., Ribas-Carbo M., Del-Saz N.F., Schwahn K., Nikoloski Z., Fernie A.R., Flexas J. (2016) Unravelling the *in vivo* regulation and metabolic role of the alternative oxidase pathway in C3 species under photoinhibitory conditions. *New Phytologist* 212: 66-79.

Gardeström P., Igamberdiev A.U. (2016) The origin of cytosolic ATP in photosynthetic cells. *Physiologia Plantarum* 157: 367-379.

Gaston S., Ribas-Carbo M., Busquets S., Berry J.A., Zabalza A., Royuela M. (2003) Changes in mitochondrial electron partitioning in response to herbicides inhibiting branched-chain amino acid biosynthesis in soybean. *Plant Physiology* 133: 1351-1359.

Geigenberger P., Thormählen I., Daloso D.M., Fernie A.R. (2017) The unprecedented versatility of the plant thioredoxin system. *Trends in Plant Science* 22: 249-262.

730 Gelhaye E., Rouhier N., Gerard J., Jolivet Y., Gualberto J., Navrot N., Ohlsson P.,
731 Wingsle G., Hirasawa M., Knaff D.B. *et al.* (2004) A specific form of thioredoxin h
732 occurs in plant mitochondria and regulates the alternative oxidase. *Proceedings of the*
733 *National Academy of Sciences of the United States of America* 101: 14545-14550.

734

735 Gray G.R., Villarimo A.R., Whitehead C.L., McIntosh L. (2004) Transgenic tobacco
736 (*Nicotiana tabacum* L.) plants with increased expression levels of mitochondrial NADP⁺-
737 dependent isocitrate dehydrogenase: evidence implicating this enzyme in the redox
738 activation of the alternative oxidase. *Plant and Cell Physiology* 45: 1413-1425.

739

740 Guy R.D., Berry J.A., Fogel M.L., Hoering T.C. (1989) Differential fractionation of
741 oxygen isotopes by cyanide-resistant and cyanide-sensitive respiration in plants. *Planta*
742 177: 483-491.

743

744 Hasse D., Andersson E., Carlsson G., Maslobov A., Hagemann M., Bauwe H., Andersson
745 I. (2013) Structure of the homodimeric glycine decarboxylase P-protein from
746 *Synechocystis* sp. PCC 6803 suggests a mechanism for redox regulation. *Journal of*
747 *Biological Chemistry* 288: 35333-35345.

748

749 Hoefnagel M.H.N., Millar A.H., Wiskich J.T., Day D.A. (1995) Cytochrome and
750 alternative respiratory pathways compete for electrons in the presence of pyruvate in
751 soybean mitochondria. *Archives of Biochemistry Biophysics* 318: 394-400.

752

753 Hoffmann C., Plochanski B., Haferkamp I., Leroch M., Ewald R., Bauwe H., Riemer J.,
754 Herrmann J.M., Neuhaus H.E. (2013) From endoplasmic reticulum to mitochondria:
755 absence of the Arabidopsis ATP antiporter endoplasmic Reticulum Adenylate
756 Transporter1 perturbs photorespiration. *Plant Cell* 25: 2647-60.

757

758 Huege J., Goetze J., Dethloff F., Junker B., Kopka J. (2014) Quantification of stable
759 isotope label in metabolites via mass spectrometry. *Methods in Molecular Biology* 1056:
760 213-223.

761

762 Igamberdiev A.U., Gardeström P. (2003) Regulation of NAD- and NADP-dependent
763 isocitrate dehydrogenases by reduction levels of pyridine nucleosides in mitochondria
764 and cytosol of pea leaves. *Biochimica et Biophysica Acta* 1606: 117-125.

765

766 Kopka J., Schauer N., Krueger S., Birkemeyer C., Usadel B., Bergmüller E., Dormann
767 P., Weckwerth W., Gibon Y., Stitt M. *et al.* (2005) GMD@CSB.DB: the Golm
768 Metabolome Database. *Bioinformatics* 21: 1635-1638.

769

770 Ku S.B., Edwards G.E. (1977) Oxygen inhibition of photosynthesis: I. Temperature
771 dependence and relation to O₂/CO₂ solubility ratio. *Plant Physiology* 59: 986-990.

772

773 Kühn K., Obata T., Feher K., Bock R., Fernie A.R., Meyer E.H. (2015) Complete
774 mitochondrial Complex I deficiency induces an up-regulation of respiratory fluxes that is
775 abolished by traces of functional Complex I. *Plant Physiology* 168: 1537-1549.

776

777 Krueger S., Niehl A., Lopez Martin M.C., Steinhauser D., Donath A., Hildebrandt T.,
778 Romero L.C., Hoefgen R., Gotor C., Hesse H. (2009) Analysis of cytosolic and plastidic
779 serine acetyltransferase mutants and subcellular metabolite distributions suggests
780 interplay of the cellular compartments for cysteine biosynthesis in *Arabidopsis*. *Plant Cell*
781 *and Environment* 32: 349-367.

782

783 Kruger N.J., Masakapalli S.K., Ratcliffe R.G. (2017) Assessing metabolic flux in plants
784 with radiorespirometry. *Methods in Molecular Biology* 1670: 1-16.

785

786 Laloi C., Rayapuram N., Chartier Y., Grienemberger J.M., Bonnard G., Meyer Y. (2001)
787 Identification and characterization of a mitochondrial thioredoxin system in plants.
788 *Proceedings of the National Academy of Sciences of the United States of America* 98:
789 14144-14149.

790

791 Lisec J., Schauer N., Kopka J., Willmitzer L., Fernie A.R. (2006) Gas chromatography
792 mass spectrometry-based metabolite profiling in plants. *Nature Protocols* 1: 387-396.

793

794 Luedemann A., Strassburg K., Erban A., Kopka J. (2008) TagFinder for the quantitative
795 analysis of gas chromatography-mass spectrometry (GC-MS)-based metabolite profiling
796 experiments. *Bioinformatics* 24: 732-737.

797

798 Marti M.C., Olmos E., Calvete J.J., Diaz I., Barranco-Medina S., Whelan J., Lazaro J.J.,
799 Sevilla F., Jimenez A. (2009) Mitochondrial and nuclear localization of a novel pea
800 thioredoxin: identification of its mitochondrial target proteins. *Plant Physiology* 150:
801 646-657.

802

803 Meng L., Wong J.H., Feldman L.J., Lemaux P.G., and Buchanan B.B. (2010) A
804 membrane-associated thioredoxin required for plant growth moves from cell to cell,
805 suggestive of a role in intercellular communication. *Proceedings of the National Academy*
806 *of Sciences of the United States of America* 107: 3900–3905.

807

808 Meyer Y., Belin C., Delorme-Hinoux V., Reichheld J.P., Riondet C. (2012) Thioredoxin
809 and glutaredoxin systems in plants: molecular mechanisms, crosstalks, and functional
810 significance. *Antioxidants and Redox Signaling* 17: 1124–1160.

811

812 Millar A.H., Wiskich J.T., Whelan J., Day D.A. (1993) Organic acid activation of the
813 alternative oxidase of plant mitochondria. *FEBS Letters* 329: 259-262.

814

815 Millar A.H., Hoefnagel M.H.N., Day D.A., Wiskich J.T. (1996) Specificity of the organic
816 acid activation of alternative oxidase in plant mitochondria. *Plant Physiology* 111: 613-
817 618.

818

819 Millenaar F.F., Gonzalez-Meler M.A., Fiorani F., Welschen R., Ribas-Carbo M., Siedow
820 J.N., Wagner A.M., Lambers H. (2001) Regulation of alternative oxidase activity in six
821 wild monocotyledonous species. An *in vivo* study at the whole root level. *Plant*
822 *Physiology* 126: 376–387.

823

824 Millenaar F.F., Lambers H. (2003) The alternative oxidase: *in vivo* regulation and
825 function. *Plant Biology* 5: 2-15.

826

827 Moore A.L., Siedow J.N. (1991) The regulation and nature of the cyanide-resistant
828 alternative oxidase of plant mitochondria. *Biochimica et Biophysica Acta* 1059: 121-140.

829

830 Moseler A., Aller I., Wagner S., Nietzel T., Przybyla-Toscano J., Mühlenhoff U., Lill R.,
831 Berndt C., Rouhier N., Schwarzländer M., Meyer A.J. (2015) The mitochondrial
832 monothiol glutaredoxin S15 is essential for iron-sulfur protein maturation in *Arabidopsis*
833 *thaliana*. *Proceedings of the National Academy of Sciences of the United States of*
834 *America* 112: 13735-13740.

835

836 Nietzel T., Mostertz J., Hochgräfe F., Schwarzländer M. (2017) Redox regulation of
837 mitochondrial proteins and proteomes by cysteine thiol switches. *Mitochondrion* 33:72-
838 83.

839

840 Noguchi K., Taylor N.L., Millar A.H., Lambers H., Day D.A. (2005) Response of
841 mitochondria to light intensity in the leaves of sun and shade species. *Plant Cell and*
842 *Environment* 28: 760-771.

843

Oliver S.N., Lunn J.E., Urbanczyk-Wochniak E., Lytovchenko A., van Dongen J.T., Faix B., Schmalzlin E., Fernie A.R., Geigenberger P. (2008) Decreased expression of cytosolic pyruvate kinase in potato tubers leads to a decline in pyruvate resulting in an *in vivo* repression of the alternative oxidase. *Plant Physiology* 148: 1640-1654.

Ortiz-Espín A., Iglesias-Fernández R., Calderón A., Carbonero P., Sevilla F., Jiménez A. (2017) Mitochondrial *AtTrxo1* is transcriptionally regulated by AtbZIP9 and AtAZF2 and affects seed germination under saline conditions. *Journal and Experimental Botany* 68: 1025–1038.

Rasmusson A.G., Fernie A.R., van Dongen J.T. (2009) Alternative oxidase: a defence against metabolic fluctuations? *Physiologia Plantarum* 137: 371-382.

Reichheld J.P., Meyer E., Khafif M., Bonnard G., Meyer Y. (2005) AtNTRB is the major mitochondrial thioredoxin reductase in *Arabidopsis thaliana*. *FEBS Letters* 579: 337-342.

Ribas-Carbo M., Berry J.A., Yakir D., Giles L., Robinson S.A., Lennon A.M., Siedow J.N. (1995) Electron partitioning between the cytochrome and alternative pathways in plant mitochondria. *Plant Physiology* 109: 829-837.

Ribas-Carbo M., Lennon A.M., Robinson S.A., Giles L., Berry J.A., Siedow J.N. (1997) The regulation of electron partitioning between the cytochrome and alternative pathways in soybean cotyledon and root mitochondria. *Plant Physiology* 113: 903-911.

Ribas-Carbo M., Robinson S.A., Giles L. (2005) The application of the oxygen-isotope technique to assess respiratory pathway partitioning. In: Lambers H, Ribas-Carbo M, eds. *Plant Respiration: From Cell to Ecosystem vol. 18. Advances in Photosynthesis and Respiration Series*. Dordrecht, The Netherlands: Springer, 31-42.

873 Riemer J., Schwarzländer M., Conrad M., Herrmann J.M. (2015) Thiol switches in
874 mitochondria: operation and physiological relevance. *Biological Chemistry* 396: 465-482.
875

876 Sánchez-Guerrero A., Del-Saz N.F., Florez-Sarasa I., Ribas-Carbó M., Fernie A.R.,
877 Jiménez A., Sevilla F. (2019) Coordinated responses of mitochondrial antioxidative
878 enzymes, respiratory pathways and metabolism in *Arabidopsis thaliana* thioredoxin *trxo1*
879 mutants under salinity. *Environmental and Experimental Botany* 162: 212–222.
880

881 Selinski J., Hartmann A., Kordes A., Deckers-Hebestreit G., Whelan J., Scheibe R. (2017)
882 Analysis of posttranslational activation of alternative oxidase isoforms. *Plant Physiology*
883 174: 2113-2127.
884

885 Sweetlove L.J., Beard K.F.M., Nunes-Nesi A., Fernie A.R., Ratcliffe R.G. (2010) Not
886 just a circle: flux modes in the plant TCA cycle. *Trends in Plant Science* 15: 462-470.
887

888 Traverso J.A., Micaella C., Martinez A., Brown S.C., Satiat-Jeunemaître B., Meinel T.,
889 Giglione C. (2013) Roles of N-Terminal fatty acid acylations in membrane compartment
890 partitioning: *Arabidopsis* h-type thioredoxins as a case study. *Plant Cell* 25: 1056–1077.
891

892 Umbach A.L., Siedow J.N. (1993) Covalent and noncovalent dimers of the cyanide-
893 resistant oxidase protein in higher plant mitochondria and their relationship to enzyme
894 activity. *Plant Physiology* 103: 845-854.
895

896 Umbach A.L., Wiskich J.T., Siedow J.N. (1994) Regulation of alternative oxidase
897 kinetics by pyruvate and intermolecular disulfide bond redox status in soybean seedling
898 mitochondria. *FEBS Letters* 348: 181-184.
899

900 Umekawa Y., Ito K. (2018) Thioredoxin o-mediated reduction of mitochondrial
 901 alternative oxidase in the thermogenic skunk cabbage *Symplocarpus renifolius*. *The*
 902 *Journal of Biochemistry*. doi: 10.1093/jb/mvy082.

903

904 Van den Ende W. (2013) Multifunctional fructans and raffinose family oligosaccharides.
 905 *Frontiers of Plant Science* 4: 247

906

907 Vanlerberghe G.C., Yip J.Y.H., Parsons H.L. (1999) *In organello* and *in vivo* evidence of
 908 the importance of the regulatory sulfhydryl/disulfide system and pyruvate for alternative
 909 oxidase activity in tobacco. *Plant Physiology* 121: 793–803.

910

911 Vanlerberghe G.C. (2013) Alternative oxidase: a mitochondrial respiratory pathway to
 912 maintain metabolic and signaling homeostasis during abiotic and biotic stress in plants.
 913 *International Journal of Molecular Sciences* 14: 6805–6847.

914

915 Yoshida K., Hisabori T. (2016) Adenine nucleotide-dependent and redox-independent
 916 control of mitochondrial malate dehydrogenase activity in *Arabidopsis thaliana*.
 917 *Biochimica et Biophysica Acta* 1857: 810-818.

918

919 Yoshida K., Noguchi K., Motohashi K., Hisabori T. (2013) Systematic exploration of
 920 thioredoxin target proteins in plant mitochondria. *Plant and Cell Physiology* 54: 875-892.

921

922 Zhang Z.S., Liu M.J., Scheibe R., Selinski J., Zhang L.T., Yang C., Meng X.L., Gao H.Y.
 923 (2017) Contribution of the alternative respiratory pathway to PSII photoprotection in C3
 924 and C4 plants. *Molecular Plant* 10: 131-142.

FIGURE LEGENDS

Figure 1. *In vivo* mitochondrial electron transport chain activities in *trxol* mutants. (A) Total respiration (V_t), (B) COX pathway activity (v_{cyt}) and (C) AOX pathway activity (v_{alt}) in leaves of *Col-0*, *trxol-1* and *trxol-2* (see Material and Methods section) *Arabidopsis thaliana* plants at moderate light (ML) and after 2 and 4 hours of high light (HL) treatment. Values are means \pm SE of five replicates. Asterisks denote significant differences ($P < 0.05$) to the ML conditions in each genotype and number symbols indicate significant difference ($P < 0.05$) to the *Col-0* in each light condition.

Figure 2. AOX capacity and protein levels in *trxol* mutants. (A) AOX capacity (V_{alt}) and (B) protein levels in leaves of *Col-0*, *trxol-1* and *trxol-2* plants at moderate light (ML) and after 2 and 4 hours of high light (HL) treatment. Values in A are means \pm SE of five replicates. In B, one representative blot is presented and the relative values shown are the mean of the four immunoblot experiments performed with similar results (Supplemental Figure S2). The relative values indicate the intensities of the signals from AOX normalized to those from porin, and then expressed as fold-changes relative to values of *Col-0* under ML intensity.

Figure 3. AOX protein redox state in *trxol* mutants. AOX protein immunodetection in leaf membranes fractions from *Col-0*, *trxol-1* and *trxol-2* plants grown under ML conditions (see Material and Methods) and treated with 50 mM DTT (for reduced-monomeric form detection) or 50 mM diamide (for oxidized-dimeric form detection) or in absence of both (-). Porin immunodetection in the same samples shows a similar mitochondrial loading among genotypes in each (redox) treatment. The table below the image shows the mean values ($n=2$) of the percentages on the oxidized and reduced forms in the different genotypes after band quantification of the blot in the current figure and in Supplemental Figure S2.

Figure 4. TCA cycle and other respiratory fluxes in *trxol* mutants. Radioactivity in the CO_2 evolved from illuminated leaf discs was measured after incubation with glucose (Glc) ^{14}C -labeled at different positions. The $^{14}\text{CO}_2$ evolution from Glc labeled at position

1 (C1) or positions 3 and 4 (C3-4) corresponds to the metabolic flux through glycolysis and TCA cycle, respectively. The $^{14}\text{CO}_2$ evolution was measured every hour after the addition of the labeled Glc and summed up to calculate the total ^{14}C evolved. Each point represent the means \pm SE of three replicates. Asterisks denote significant differences ($P < 0.05$) to the *Col-0* plants in each time point.

Figure 5. Photosynthetic and photorespiratory parameters under high light stress conditions. Net photosynthesis (A_N), photosynthetic electron transport rate (ETR), stomatal conductance (g_s) and the percentage of O_2 inhibition of photosynthesis in leaves in *Col-0*, *trxo1-1* and *trxo1-2* plants grown under ML and after 2 and 4h of high light (HL) treatment. Details on the gas exchange and chlorophyll fluorescence measurements can be found in the Material and Methods section. Values are means \pm SE of six (A_N , g_s and ETR) or four (% O_2 inhibition) replicates and asterisks denote significant differences ($P < 0.05$) to the *Col-0* plants in each light condition.

Figure 6. Metabolite profiling in *trxo1* mutants. Heat map showing the relative levels of the GC-MS-analyzed metabolites in *Col-0*, *trxo1-1* and *trxo1-2* plants grown under ML and after 2 and 4h of high light (HL) treatment. Metabolites were clustered per class into amino acids, organic acids, sugars and sugar alcohols, and other metabolites. Relative metabolite levels in leaves of *Col-0*, *trxo1-1* and *trxo1-2* plants under all light conditions were normalized to the mean level of the *Col-0* plants under ML conditions and fold-change values were log2 transformed (i.e. the level of all metabolites of *Col-0* plants under ML is 0). In this heat map, red and blue colors represent log2 fold-increased and -decreased metabolites, respectively. Values are means \pm SE of six replicates and asterisks denote significant differences ($P < 0.05$) to the *Col-0* plants in each light condition. The statistical differences between ML and HL treatments in each genotype are presented in Supplemental Table S2.

Figure 7. Total ^{13}C label redistribution into primary metabolites in *trxo1* mutants. The total ^{13}C label redistribution in selected leaf metabolites of *Col-0*, *trxo1-1* and *trxo1-2* plants was determined after 2 and 4 hours of ^{13}C -labeling under (A) moderate light and

(B) high light conditions. Values are means \pm SE of six replicates and asterisks denote significant differences ($P < 0.05$) to the *Col-0* plants in each time point and light condition. Only metabolites showing significant differences to the *Col-0* in both mutant lines in each light treatment, considering all time points and labeling substrates, are shown. Data including total ^{13}C label redistribution in all metabolites is presented in Supplemental Table S3 and Table S4.

SUPPORTING INFORMATION

Supplemental Table S1. Parameters used for peak annotation in GC-MS analysis.

Supplemental Table S2. Relative metabolite levels in leaves of *Col-0*, *trxo1-1* and *trxo1-2* plants under moderate light (ML) and after 2 and 4h of high light (HL) treatment. Data is presented as means \pm SE for six biological replicates normalized to the mean level of the *Col-0* plants under ML. Bold numbers denote significant differences ($P < 0.05$) to the ML conditions in each genotype and asterisks indicate significant difference ($P < 0.05$) to the *Col-0* in each light condition.

Supplemental Table S3. Total ^{13}C label redistribution in leaf metabolites of *Col-0*, *trxo1-1* and *trxo1-2* plants after 2 and 4 hours of ^{13}C -Glucose labeling under moderate light and high light conditions. Values are means \pm SE of six replicates, and those values bold and underlined denote significant differences ($P < 0.05$) to the *Col-0* plants in each time point and light condition.

Supplemental Table S4. Total ^{13}C label redistribution in leaf metabolites of *Col-0*, *trxo1-1* and *trxo1-2* plants after 2 and 4 hours of ^{13}C -Malate labeling under moderate light and high light conditions. Values are means \pm SE of six replicates, and those values bold and underlined denote significant differences ($P < 0.05$) to the *Col-0* plants in each time point and light condition.

Supplemental Table S5. Primers used in the qPCR analyses performed in this study.

Supplemental Figure S1. Gene expression analysis and biomass accumulation of *trxo1* mutants. (A) qPCR analysis of transcript levels from genes related to mitochondrial TRX system and *AOX1a* in leaves *trxo1-1* and *trxo1-2* plants under moderate light conditions (ML). Primers used and gene information can be found in Supplemental Table S5. Values are means \pm SE of 4 replicates and asterisks denote significant differences ($P < 0.05$) to

the *Col-0* plants; n.d. (not detected). (B) Photograph representative of *Col-0*, *trxo1-1* and *trxo1-2* plants after growing for 6 weeks under ML conditions. (C) Rosette biomass accumulation of plants grown as in B. Values are means \pm SE of twelve replicates and asterisks denote significant differences ($P < 0.05$) to the *Col-0* plants.

Supplemental Figure S2. AOX protein amount and redox analysis. (A) AOX and porin protein levels in leaves of *Col-0*, *trxo1-1* and *trxo1-2* plants at moderate light (ML) and after 2 and 4 hours of high light (HL) treatment. Three blots of each AOX and porin proteins are shown, which were used for the AOX amount quantifications, together with the blot shown in Figure 2B, as described in Material and Methods section. (B) AOX protein redox state in *trxo1* mutants. AOX protein immunodetection in leaf membranes fractions from *Col-0*, *trxo1-1* and *trxo1-2* plants grown under ML conditions (see Material and Methods) and treated with 50 mM DTT (for reduced-monomeric form detection) or 50 mM diamide (for oxidized-dimeric form detection) or in absence of both (-).

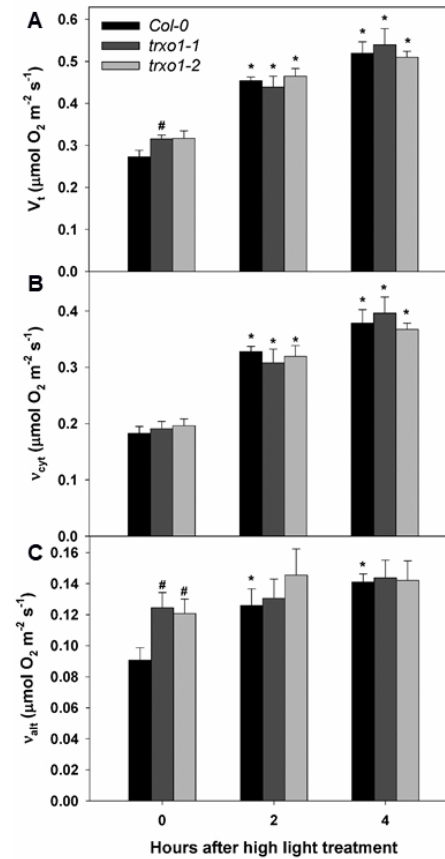
Figure 1

Figure 1. In vivo mitochondrial electron transport chain activities in *trxo1* mutants. (A) Total respiration (V_t), (B) COX pathway activity (V_{cyt}) and (C) AOX pathway activity (V_{alt}) in leaves of *Col-0*, *trxo1-1* and *trxo1-2* (see Experimental Procedures) *Arabidopsis thaliana* plants at growth light (GL) and after 2 and 4 hours of high light (HL) treatment. Values are means \pm SE of five replicates. Asterisks denote significant differences ($P < 0.05$) to the GL conditions in each genotype and number symbols indicate significant difference ($P < 0.05$) to the *Col-0* in each light condition.

190x275mm (96 x 96 DPI)

Figure 2

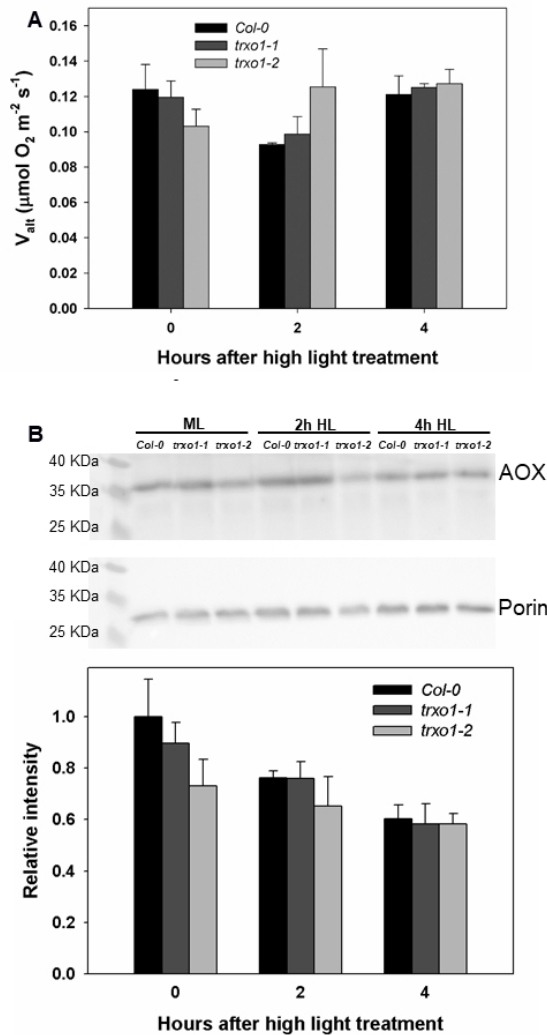


Figure2. AOX capacity and protein levels in *trxo1* mutants. (A) AOX capacity (V_{alt}) and (B) protein levels in leaves of Col-0, *trxo1-1* and *trxo1-2* plants at moderte light (ML) and after 2 and 4 hours of high light (HL) treatment. Values in A are means \pm SE of five replicates. In B, one representative blot is presented and the relative values shown are the mean of the four immunoblot experiments performed with similar results (Supplemental Figure S2). The relative values indicate the intensities of the signals from AOX normalized to those from porin, and then expressed as fold-changes relative to values of Col-0 under ML intensity.

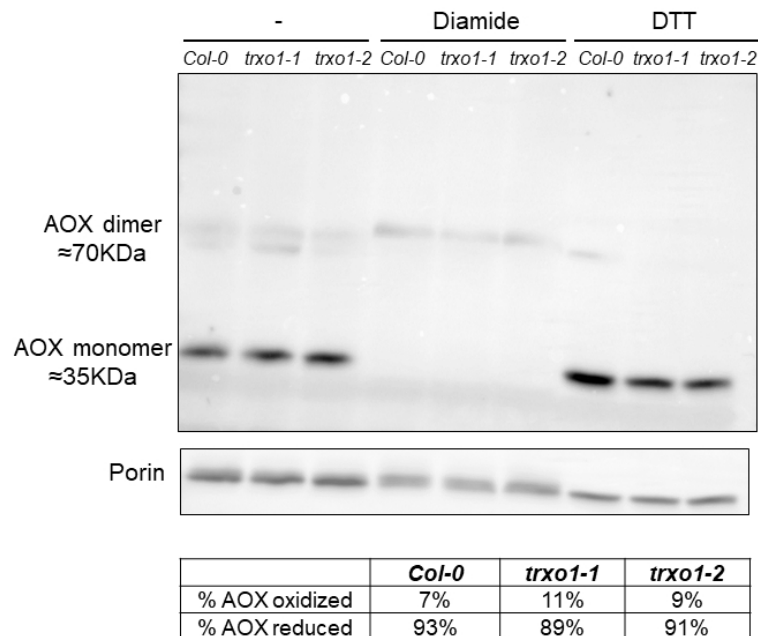
Figure 3

Figure 3. AOX protein redox state in *trxo1* mutants. AOX protein immunodetection in leaf membranes fractions from *Col-0*, *trxo1-1* and *trxo1-2* plants grown under ML conditions (see Material and Methods) and treated with 50 mM DTT (for reduced-monomeric form detection) or 50 mM diamide (for oxidized-dimeric form detection) or in absence of both (-). Porin immunodetection in the same samples shows a similar mitochondrial loading among genotypes in each (redox) treatment. The table below the image shows the mean values (n=2) of the percentages on the oxidized and reduced forms in the different genotypes after band quantification of the blot in the current figure and in Supplemental Figure S2.

190x275mm (96 x 96 DPI)

Figure 4

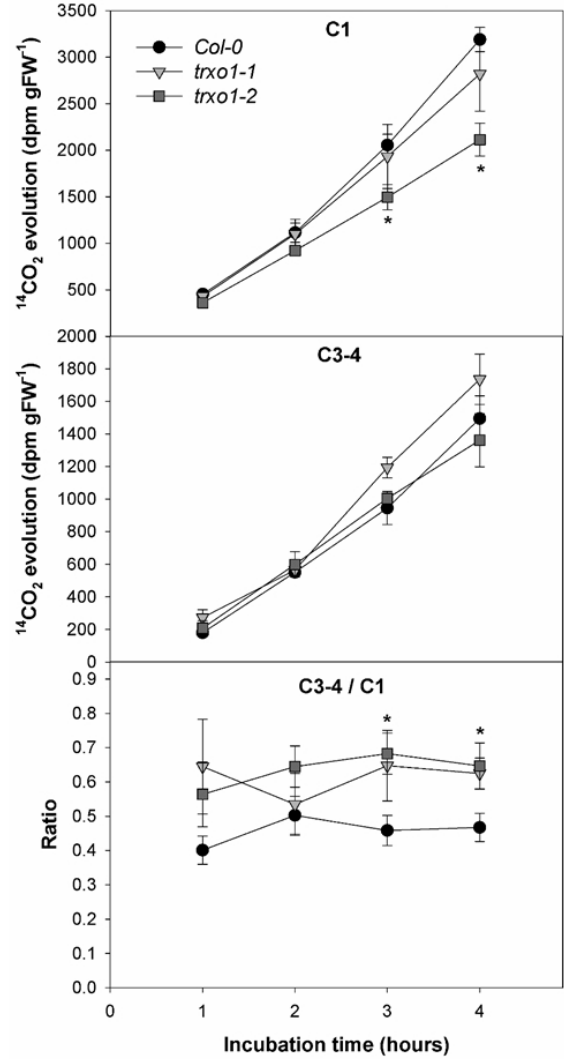


Figure 4. TCA cycle and other respiratory fluxes in *trxo1* mutants. Radioactivity in the CO_2 evolved from illuminated leaf discs was measured after incubation with glucose (Glc) ^{14}C -labeled at different positions. The $^{14}\text{CO}_2$ evolution from Glc labeled at position 1 (C1) or positions 3 and 4 (C3-4) corresponds to the metabolic flux through glycolysis and TCA cycle, respectively. The $^{14}\text{CO}_2$ evolution was measured every hour after the addition of the labeled Glc and summed up to calculate the total ^{14}C evolved. Each point represent the means \pm SE of three replicates. Asterisks denote significant differences ($P < 0.05$) to the *Col-0* plants in each time point.

190x275mm (96 x 96 DPI)

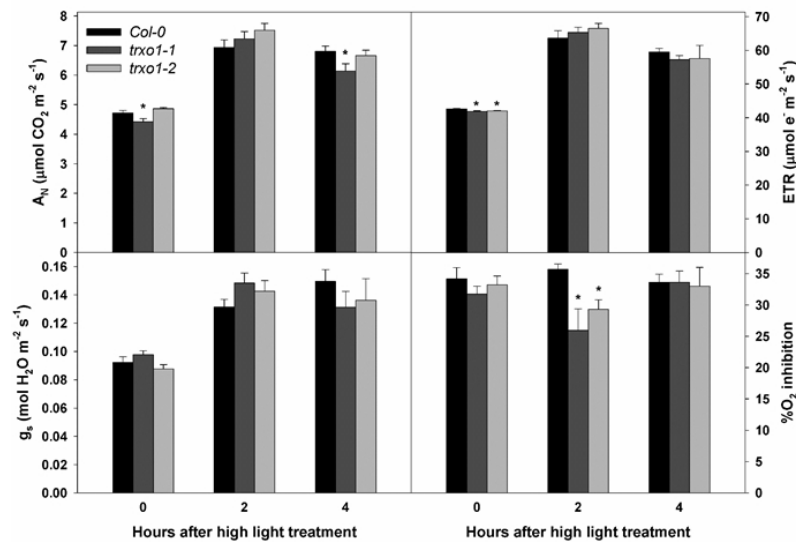
Figure 5

Figure 5. Photosynthetic and photorespiratory parameters under high light stress conditions. Net photosynthesis (A_N), photosynthetic electron transport rate (ETR), stomatal conductance (g_s) and the percentage of O₂ inhibition of photosynthesis in leaves in Col-0, trxo1-1 and trxo1-2 plants grown under GL and after 2 and 4h of high light (HL) treatment. Details on the gas exchange and chlorophyll fluorescence measurements can be found in the Experimental Procedures section. Values are means \pm SE of six (A_N , g_s and ETR) or four (% O₂ inhibition) replicates and asterisks denote significant differences ($P < 0.05$) to the Col-0 plants in each light condition.

190x275mm (96 x 96 DPI)

Figure 6

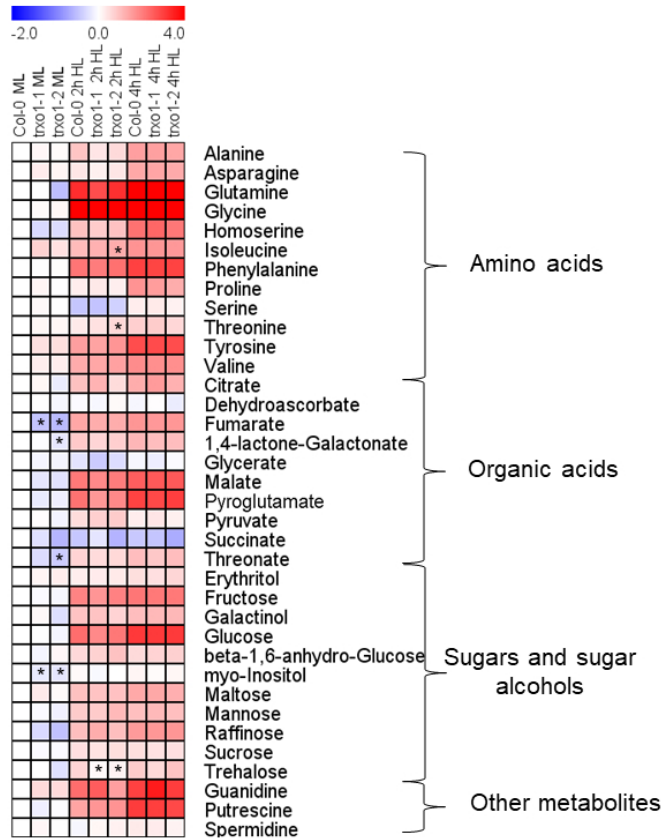


Figure 6. Metabolite profiling in *trxo1* mutants. Heat map showing the relative levels of the GC-MS-analyzed metabolites in Col-0, *trxo1-1* and *trxo1-2* plants grown under ML and after 2 and 4h of high light (HL) treatment. Metabolites were clustered per class into amino acids, organic acids, sugars and sugar alcohols, and other metabolites. Relative metabolite levels in leaves of Col-0, *trxo1-1* and *trxo1-2* plants under all light conditions were normalized to the mean level of the Col-0 plants under ML conditions and fold-change values were log2 transformed (i.e. the level of all metabolites of Col-0 plants under ML is 0). In this heat map, red and blue colors represent log2 fold-increased and -decreased metabolites, respectively. Values are means \pm SE of six replicates and asterisks denote significant differences ($P < 0.05$) to the Col-0 plants in each light condition. The statistical differences between ML and HL treatments in each genotype are presented in Supplemental Table S2.

Figure 7

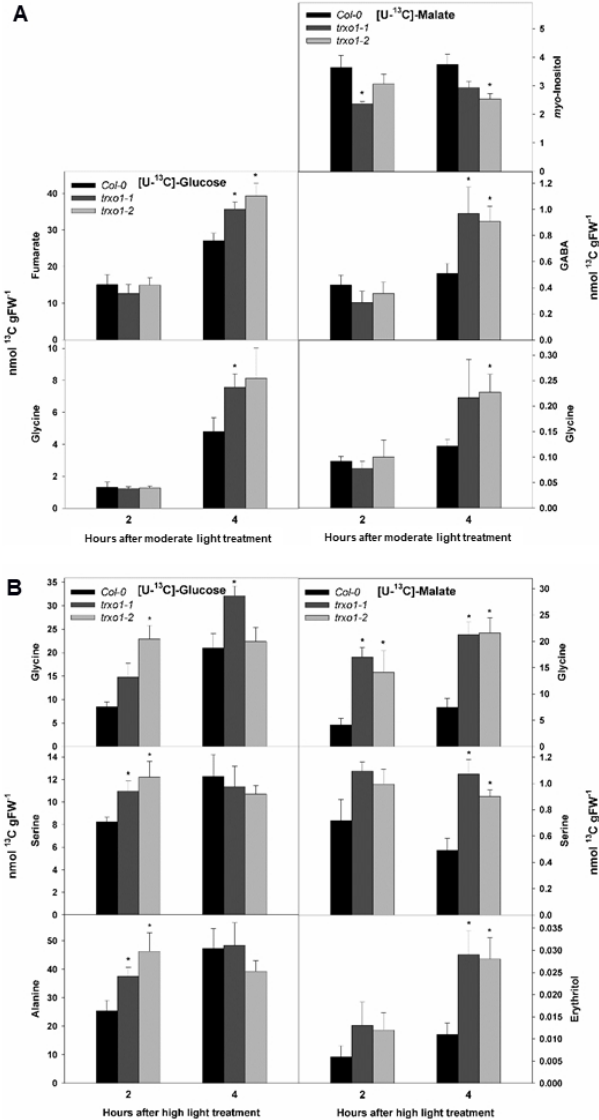


Figure 7. Total ^{13}C label redistribution into primary metabolites in *trxo1* mutants. The total ^{13}C label redistribution in selected leaf metabolites of *Col-0*, *trxo1-1* and *trxo1-2* plants was determined after 2 and 4 hours of ^{13}C -labeling under (A) moderate light and (B) high light conditions. Values are means \pm SE of six replicates and asterisks denote significant differences ($P < 0.05$) to the *Col-0* plants in each time point and light condition. Only metabolites showing significant differences to the *Col-0* in both mutant lines in each light treatment, considering all time points and labeling substrates, are shown. Data including total ^{13}C label redistribution in all metabolites is presented in Supplemental Table S3 and Table S4.

190x275mm (96 x 96 DPI)